



Article

# Tailoring the Morphology of Monodisperse Mesoporous Silica Particles Using Different Alkoxysilanes as Silica Precursors

Fabio Fait<sup>1,2</sup>, Stefanie Wagner<sup>1</sup>, Julia C. Steinbach<sup>1,2</sup> , Andreas Kandelbauer<sup>2,3</sup> and Hermann A. Mayer<sup>1,\*</sup>

<sup>1</sup> Institute of Inorganic Chemistry, University of Tübingen, Auf der Morgenstelle 18, 72076 Tübingen, Germany; fabio.fait@reutlingen-university.de (F.F.); stefaniewagnersb@googlemail.com (S.W.); julia.steinbach@reutlingen-university.de (J.C.S.)

<sup>2</sup> Process Analysis and Technology (PA&T), Reutlingen Research Institute, Reutlingen University, Alteburgstrasse 150, 72762 Reutlingen, Germany; andreas.kandelbauer@reutlingen-university.de

<sup>3</sup> Institute of Wood Technology and Renewable Materials, Department of Material Sciences and Process Engineering (MAP), University of Natural Resources and Life Sciences, Gregor-Mendel-Strasse 33, 1180 Vienna, Austria

\* Correspondence: hermann.mayer@uni-tuebingen.de

**Abstract:** The hard template method for the preparation of monodisperse mesoporous silica microspheres (MPSMs) has been established in recent years. In this process, in situ-generated silica nanoparticles (SNPs) enter the porous organic template and control the size and pore parameters of the final MPSMs. Here, the sizes of the deposited SNPs are determined by the hydrolysis and condensation rates of different alkoxysilanes in a base catalyzed sol–gel process. Thus, tetramethyl orthosilicate (TMOS), tetraethyl orthosilicate (TEOS), tetrapropyl orthosilicate (TPOS) and tetrabutyl orthosilicate (TBOS) were sol–gel processed in the presence of amino-functionalized *poly* (glycidyl methacrylate-*co*-ethylene glycol dimethacrylate) (*p*(GMA-*co*-EDMA)) templates. The size of the final MPSMs covers a broad range of 0.5–7.3  $\mu\text{m}$  and a median pore size distribution from 4.0 to 24.9 nm. Moreover, the specific surface area can be adjusted between 271 and 637  $\text{m}^2 \text{g}^{-1}$ . Also, the properties and morphology of the MPSMs differ according to the SNPs. Furthermore, the combination of different alkoxysilanes allows the individual design of the morphology and pore parameters of the silica particles. Selected MPSMs were packed into columns and successfully applied as stationary phases in high-performance liquid chromatography (HPLC) in the separation of various water-soluble vitamins.

**Keywords:** mesoporous silica microspheres (MPSMs); hard template method; high-performance liquid chromatography (HPLC)



**Citation:** Fait, F.; Wagner, S.; Steinbach, J.C.; Kandelbauer, A.; Mayer, H.A. Tailoring the Morphology of Monodisperse Mesoporous Silica Particles Using Different Alkoxysilanes as Silica Precursors. *Int. J. Mol. Sci.* **2023**, *24*, 11729. <https://doi.org/10.3390/ijms241411729>

Academic Editor: Marina G. Shelyapina

Received: 13 June 2023  
Revised: 17 July 2023  
Accepted: 19 July 2023  
Published: 21 July 2023



**Copyright:** © 2023 by the authors. Licensee MDPI, Basel, Switzerland. This article is an open access article distributed under the terms and conditions of the Creative Commons Attribution (CC BY) license (<https://creativecommons.org/licenses/by/4.0/>).

## 1. Introduction

The introduction of high-performance liquid chromatography (HPLC) has enabled a rapid chemical analysis and separation process for substances and end products. The wide range of applications extends from small molecules [1–3] to pharmaceuticals [4,5], food and environmental analysis [6–8], long-chain polymers [9,10] and biomolecules [11–13]. The most common material in HPLC columns are spherical silica particles because of their mechanical robustness. Moreover, silica particles possess reactive groups on their surface, by which a variety of functionalizations allow a fine tuning of the particle features [14–16]. Characteristics such as particle size, dispersity, pore structure and surface functionalization influence their chromatographic properties such as selectivity, analysis time, plate number and back pressure. Due to their high specific surface area, fully porous silica particles in the  $\mu\text{m}$  range have proven successful in HPLC [17–19].

Probably the best-known representation of spherical silica networks is the silica material obtained from the Stober process [20]. Non-porous spherical silica particles in the

range of 10 to 500 nm can be formed by ammonia-catalyzed hydrolysis and the condensation of molecular alkoxy silanes. With semi-batch processes and the addition of electrolytes, the particle size can be increased into the  $\mu\text{m}$  range [21–24].

The hydrolysis rates of the alkoxy silanes are crucial for the size of the siloxane network. The hydrolysis rates are controlled by different parameters like the temperature; the chain length and branching of the alkoxy silane;  $\text{NH}_3$  and  $\text{H}_2\text{O}$  concentrations; and the chain length and branching of the alcohol, which is used as a solvent [20,25–29]. Under basic conditions, an increase in the chain length of the alkyl groups of the alkoxy silane leads to a decrease in the rate of hydrolysis. The increasing steric hindrance and inductive effects of the alkyl groups increase the electron density at the silicon atom and make a nucleophilic attack more difficult. In addition, the decreasing polarity of the alkoxy silanes can lead to phase separation, depending on the solvent applied [29–32]. The  $\text{NH}_3$  and  $\text{H}_2\text{O}$  concentrations influence the equilibrium reactions of hydrolysis and condensation. While under basic conditions the condensation of hydrolyzed alkoxy silanes is extremely fast, higher concentrations of  $\text{H}_2\text{O}$  affect the hydrolysis positively but the condensation negatively [28,29,31,33,34]. Overall, the Stober process provides non-porous silica nanoparticles with narrow size distributions. However, the preparation of monodisperse silica particles in the micrometer range is challenging, and the obtained particles remain nonporous.

The preparation of mesoporous silica microspheres (MPSMs) with narrow size distributions remains challenging [35–40]. Recently, for the synthesis of MPSMs, a promising protocol has been developed that employs functionalized porous *poly* (glycidyl methacrylate-co-ethylene glycol dimethacrylate) polymer particles (*p*(GMA-co-EDMA)) as hard templates in the presence of the basic hydrolysis and condensation of TEOS [35]. *p*(GMA-co-EDMA) functionalized with trimethylamine, (3-amino propyl) triethoxy silane or tetra ethylene pentamine (TEPA) provides excellent environments to deposit silica nanoparticles (SNPs) in the pores of the template, where they form a silica network [36–38]. The best matches of the templates are achieved if the rate of the growth of the SNPs and their rate of diffusion into the template pores are well balanced. Moreover, the particle and pore properties correlate with the size of the SNPs, which depends on the sol–gel conditions (see above) and the template [39,40].

In this study, we focus on the sol–gel conditions during the formation of MPSMs via the hard template method. Therefore, we investigated the influence of alkoxy silane precursors, which differ in their rates of hydrolysis on the particle and pore properties of MPSMs. For this, the sol–gel process of the precursors is carried out under basic conditions in the presence of the tetraethylenepentamine-functionalized *p*(GMA-co-EDMA) template P@TEPA (Scheme 1). The size of the silica nanoparticles that accumulate in and on the template depends on the hydrolysis rate of the precursors. The *p*(GMA-co-EDMA)/ $\text{SiO}_2$  hybrid beads (HB) and the MPSMs are characterized for their particles and pore properties by scanning electron microscopy, thermogravimetric analysis, and nitrogen adsorption/desorption measurements. Finally, selected MPSMs are functionalized with trimethoxy (octadecyl) silane and applied as stationary phases in the separation of different water-soluble vitamins.



by 0.7  $\mu\text{m}$  and **HB2b** by 0.3  $\mu\text{m}$  and are thus larger than **HB1a-d**. In contrast to particles prepared by Method 1, a more edgy morphology of the hybrid materials is achieved. For TPOS (**HB2c**) and TBOS (**HB2d**) as precursors, there are no changes in size and morphology compared to the template.

**Table 1.** Particle properties of hybrid beads and corresponding mesoporous silica microspheres.

	Particle Size	SiO <sub>2</sub> Content		Particle Size	Median Pore Size	Pore Volume	Specific Surface Area
	( $\mu\text{m}$ )	(%)		( $\mu\text{m}$ )	(nm)	(mL g <sup>-1</sup> )	(m <sup>2</sup> g <sup>-1</sup> )
HB1a	6.3	37.8	MPSM1a	6.0	23.6	0.50	271
HB1b	6.3	29.9	MPSM1b	5.5	11.3	0.84	389
HB1c	6.3	17.7	MPSM1c	3.6	8.8	0.62	339
HB1d	6.3	6.6	MPSM1d	2.2	4.0	0.68	637
HB2a	6.7	32.7	MPSM2a	5.9	15.7	0.87	390
HB2b	6.2	35.8	MPSM2b	6.0	24.9	0.69	346
HB2c	6.0	0.01	MPSM2c	0.8	1	1	1
HB2d	6.0	0.01	MPSM2d	0.5	1	1	1
HB1e	7.1	43.0	MPSM1e	7.3	16.6	0.79	247
HB1f	8.6	33.8	MPSM1f	6.6	15.6	1.06	311

<sup>1</sup> The poor yield did not allow us to record adsorption/desorption measurements.

The thermal degradation behavior of the hybrid beads **HB1a-d** and **HB2a-d** compares well with that reported earlier (Figure 1) [41]. After the loss of surface water, the degradation processes of the polymer backbone led to a complete decomposition of the template and allowed the determination of the silica content of the hybrid beads. Here the hybrid particles **HB1a** contain the highest quantity of silica (37.8 %). The amounts of silica of **HB1b** (29.9%), **HB1c** (17.7%) and **HB1d** (6.6%) correlate with their decreasing hydrolysis rates. The amounts of SiO<sub>2</sub> in **HB2a** and **HB2b** (32.7% and 35.8%, respectively) differ little (Figure 1). Due to the suppressed hydrolysis in H<sub>2</sub>O, the hydrolysis rates of TMOS and TEOS are comparable. Thus, similar amounts of SiO<sub>2</sub> are deposited. The percentage of incorporated silica in the hybrid particles correlates well with the particle size of the resulting MPSMs (Table 1). Thermogravimetric analyses of **HB2c** and **HB2d** result in only very small amounts of SiO<sub>2</sub>. This is traced back to the poor miscibility of the alkoxysilanes TPOS and TBOS with water. Thus, only small amounts of SNPs are generated during the reaction.

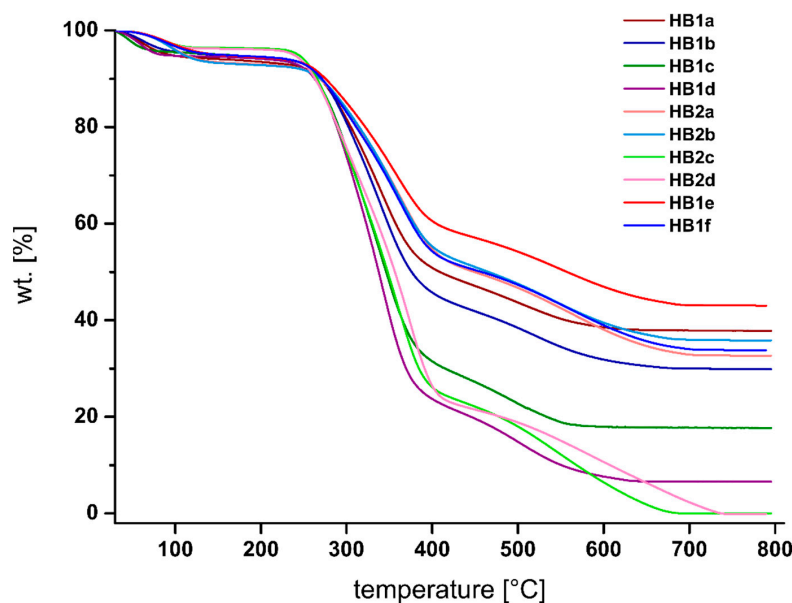


**Figure 1.** TGA measurements of hybrid beads **HB1a-f** and **HB2a-d**.

The calcination of the hybrid beads **HB1a-d** and **HB2a-d** for 10 h at 600 °C removed the organic polymer template and released the monodisperse mesoporous silica microspheres **MPSM1a-d** (Figure 2) and **MPSM2a-d** (Figure 3). The nanoparticulate morphology of the MPSMs is comparable to that of their corresponding hybrid beads. The particle size of the MPSMs decreases with the decreasing hydrolysis rate of the precursors. Thus, while **MPSM1a** (6.0  $\mu\text{m}$ ) and **MPSM1b** (5.5  $\mu\text{m}$ ) represent the size of the template quite well, the sizes of **MPSM1c** (3.6  $\mu\text{m}$ ) and **MPSM1d** (2.2  $\mu\text{m}$ ) are strongly reduced. Consequently, only TMOS and TEOS map the template to 100% and 92%, respectively, while, for TPOS and TBOS, the template is mapped to only 60% and 37%, respectively. The particle sizes of **MPSM2a** and **MPSM2b** are 5.9  $\mu\text{m}$  and 6.0  $\mu\text{m}$ , respectively, and completely replicate the template. For **MPSM2c** and **MPSM2d**, 800 nm and 500 nm polydisperse porous silica particles are generated.

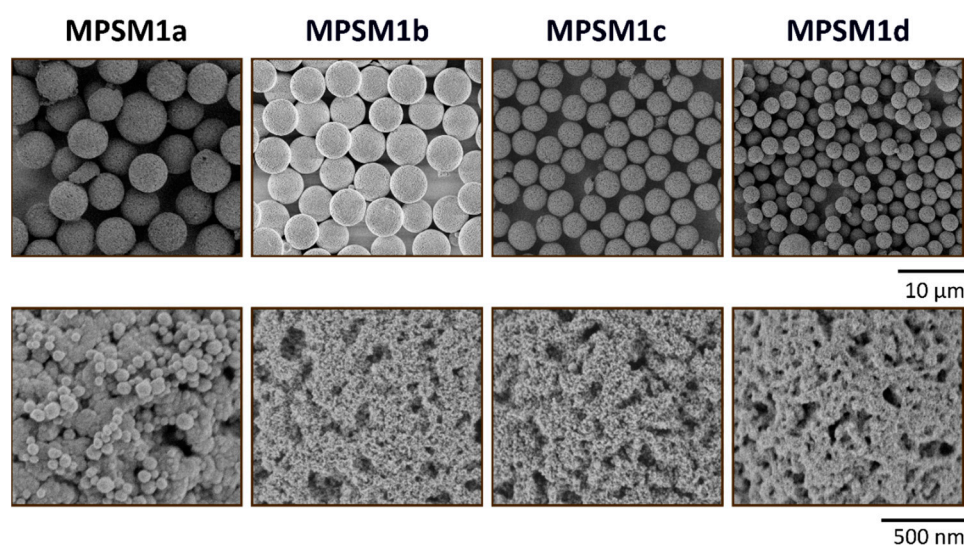


**Figure 2.** SEM images of mesoporous silica microspheres **MPSM1a-d** with 2000 $\times$  magnification (**top row**) and 50,000 $\times$  magnification (**bottom row**).

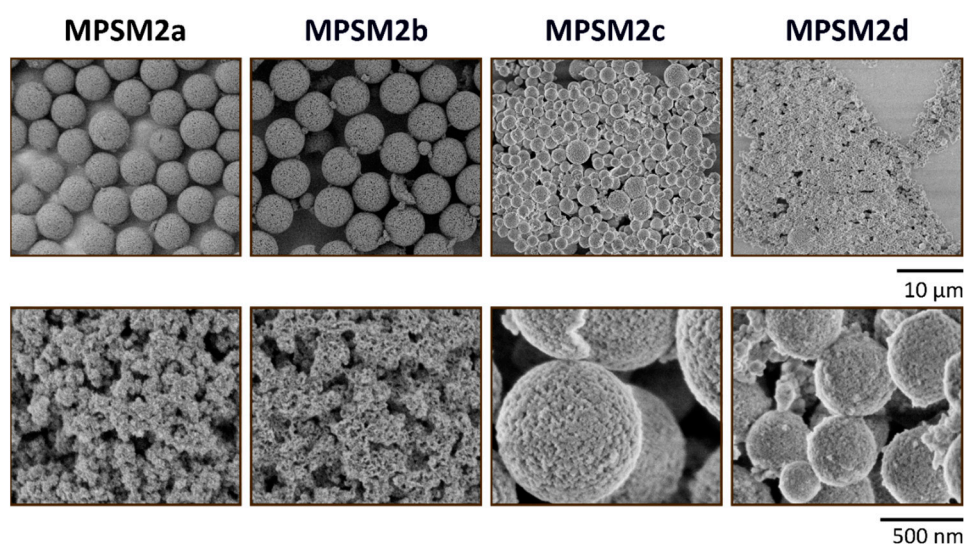


**Figure 3.** SEM images of mesoporous silica microspheres **MPSM2a-d** with 2000 $\times$  magnification (**top row**) and 50,000 $\times$  magnification (**bottom row**).

The pore properties of the MPSMs were determined via nitrogen adsorption/desorption measurements and are listed in Table 1. The corresponding pore size distributions are shown in Figure 4. Here, the median pore size of the MPSMs decreases and the specific

surface area increases with the decreasing hydrolysis rates of the precursors. This result is consistent with the size of the SNPs that form the silica network. Large SNPs generate large pores of the MPSMs, while small SNPs result in smaller pores [38,40]. Therefore, the median pore size becomes smaller in the order of **MPSM1a** (23.6 nm), **MPSM1b** (11.3 nm), **MPSM1c** (8.8 nm), and **MPSM1d** (4.0 nm). As smaller pores form larger specific surface areas, the highest specific surface area is obtained for **MPSM1d**, and the lowest specific surface area is obtained for **MPSM1a**. The sol–gel process according to Method 2 leads to an edgier morphology for **MPSM2a** and **MPSM2b**, resulting in larger surface areas compared to **MPSM1a** and **MPSM1b**. The pore volume of the MPSMs differs between  $0.5 \text{ mL g}^{-1}$  and  $0.9 \text{ mL g}^{-1}$ .

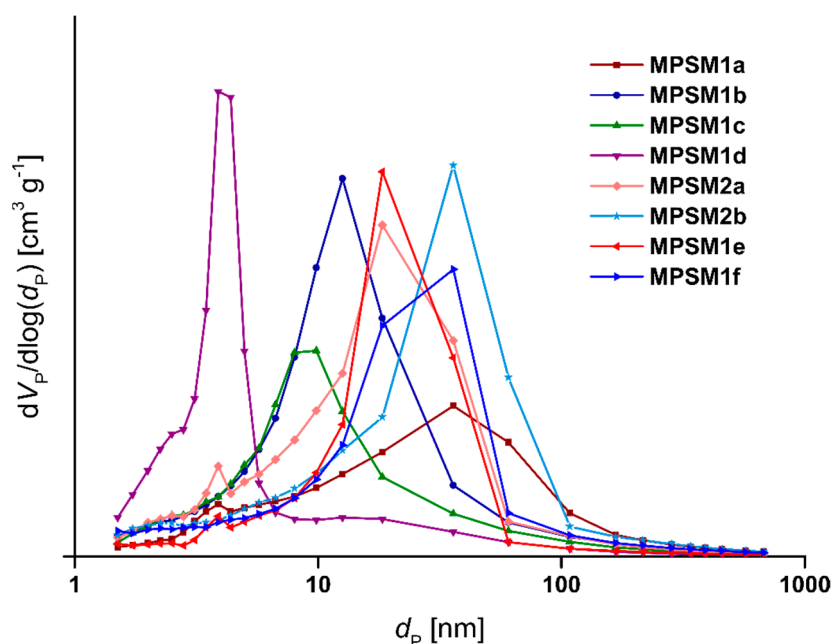


**Figure 4.** Pore size distributions of MPSM1a-f and MPSM2a-b.

## 2.2. Preparation and Characterization of MPSM1e and MPSM1f

The properties of the MPSMs are controlled by the hydrolysis rate of the precursors and the solvent medium. TMOS produces non-porous secondary particles while TPOS does not fully map the size of the template if the sol–gel process is carried out in 2-propanol and  $\text{H}_2\text{O}$ . To avoid this unwanted behavior, the two precursor combinations of TMOS with TEOS (**MPSM1e**) and TPOS with TEOS (**MPSM1f**) were applied in a sol–gel process in the presence of a P@TEPA template with a diameter of  $7.2 \mu\text{m}$ . The new HBs and MPSMs are shown in Figure 5. Interestingly, no secondary particles are observed for **HB1e** and **MPSM1e**. The **HB1e** particles have the highest silica content of all hybrid particles, and the corresponding silica microspheres have a nanoparticulate surface and exhibit a size of  $7.3 \mu\text{m}$  (Table 1). Thus, they completely map the template without the negative effects of the high hydrolysis rate of TMOS. With a median pore size of 16.6 nm, this is in between that of **MPSM1a** and **MPSM1b**. This results in SNPs in the continuous phase that are smaller than those of **MPSM1a** and larger than those of **MPSM1b**. The combination of TEOS and TPOS leads to the particles **HB1f** and **MPSM1f**. The resulting silica materials have a size of  $6.6 \mu\text{m}$ , representing 92% of the template. Interestingly, the median pore size of 15.6 nm and the pore volume of  $1.06 \text{ mL g}^{-1}$  are larger than the pore properties of **MPSM1b**, for which only TEOS was used. Compared with **MPSM1c**, the template is better replicated in **MPSM1f**.

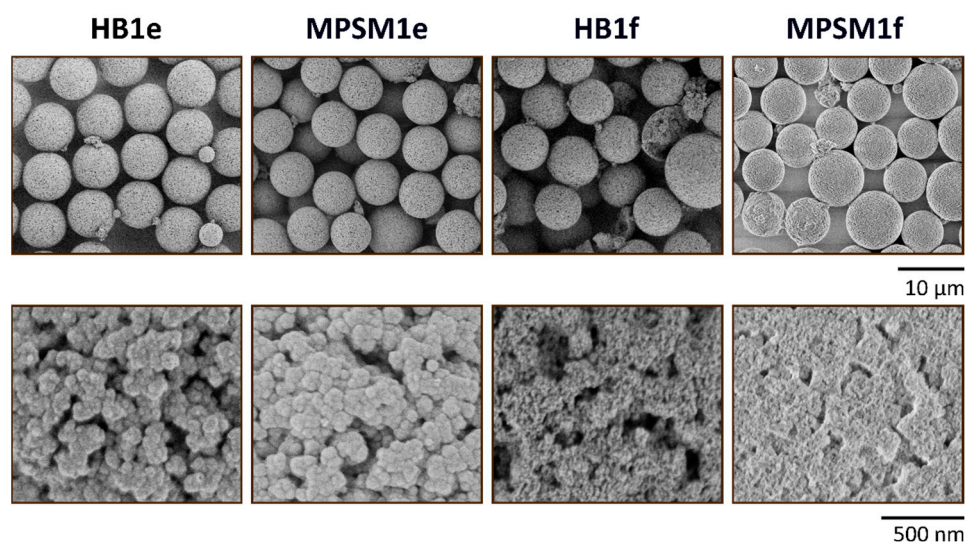


**Figure 5.** SEM images of hybrid beads **HB1e** and **HB1f** and corresponding **MPSM1e** and **MPSM1f** with 2000× magnification (**top row**) and 50,000× magnification (**bottom row**).

### 2.3. Chromatographic Measurements of **MPSM1b**

For the use of MPSMs as a stationary phase in high-performance liquid chromatography, high monodispersity is required to achieve efficient separation. **MPSM1b** particles were chosen based on their particle size and monodispersity to investigate their suitability as a stationary phase in HPLC. Therefore, **MPSM1b** particles were functionalized with trimethoxy (octadecyl) silane and packed in a 250 mm × 4.6 mm stainless steel column with acetone as the slurry and methanol/water (85 v.%/15 v.%) as the pressure medium.

The reproducibility of the synthesis of **MPSM1b** in its chromatographic properties is shown in Figure 6. The particles of three different batches with the same reaction conditions were packed in 250 mm × 4.6 mm stainless steel columns and examined for their chromatographic properties. As can be seen in Figure 6, the particles of all three batches show the same retention behavior of the test mixture. Moreover, even after one hundred injections, the retention times of toluene and uracil did not change (Supporting Information Table S1). This indicates the good stability of the stationary phase **MPSM1b-C<sub>18</sub>**.

The successful separation of five water-soluble vitamins is shown in Figure 7. A gradient from eluent A, consisting of water containing 0.025% TFA, to eluent B, consisting of acetonitrile (ACN), was used for the separation. An initial isocratic step for five minutes with eluent A is followed by an increase from eluent B to eluent A to 25/75 (v.%/v.%) in six minutes, as proposed by Heudi et al. [42]. This is followed by a second gradient on eluent B to eluent A 40/60 (v.%/v.%) in eight minutes, holding this for an additional minute. Then, the initial conditions are restored in one minute and equilibrated for four minutes. The vitamins were baseline separated and assigned based on single measurements of the analytes. The elution order is vitamin  $B_1 < B_3 < B_5 < B_9 < B_{12}$  as detected at 210 nm.

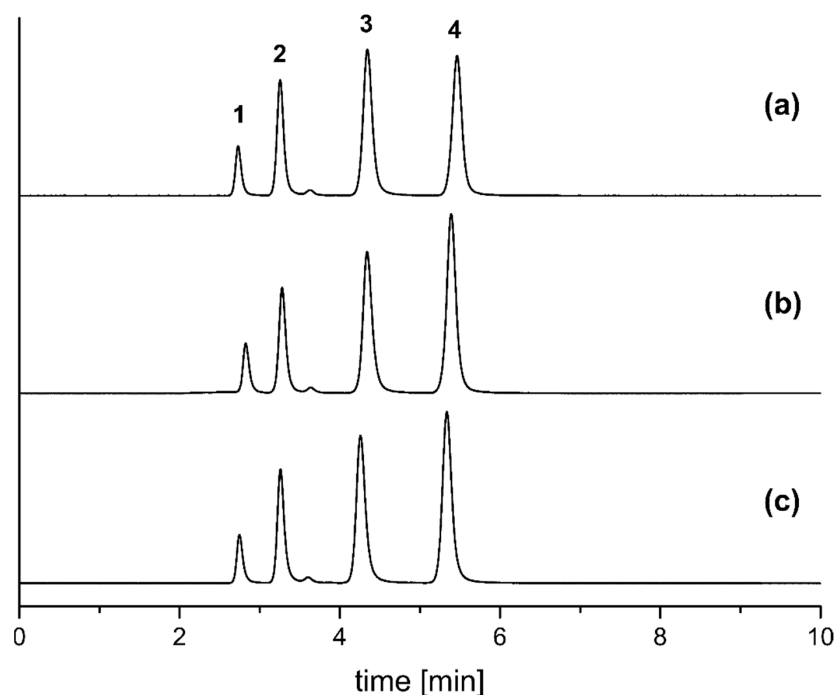


**Figure 6.** Reproducibility of chromatographic properties from three different batches (a–c) of **MPSM1b-C<sub>18</sub>** synthesized according to Method 1. Chromatographic settings: column dimension: 250 × 4.6 mm; mobile phase: MeOH/H<sub>2</sub>O (85 v.%/15 v.%); analytes: uracil (1), phenol (2), *N,N*-diethyl-*m*-toluamide (3) and toluene (4); flow: 1 mL min<sup>-1</sup>; injection volume: 5 μL; UV detection: 254 nm.

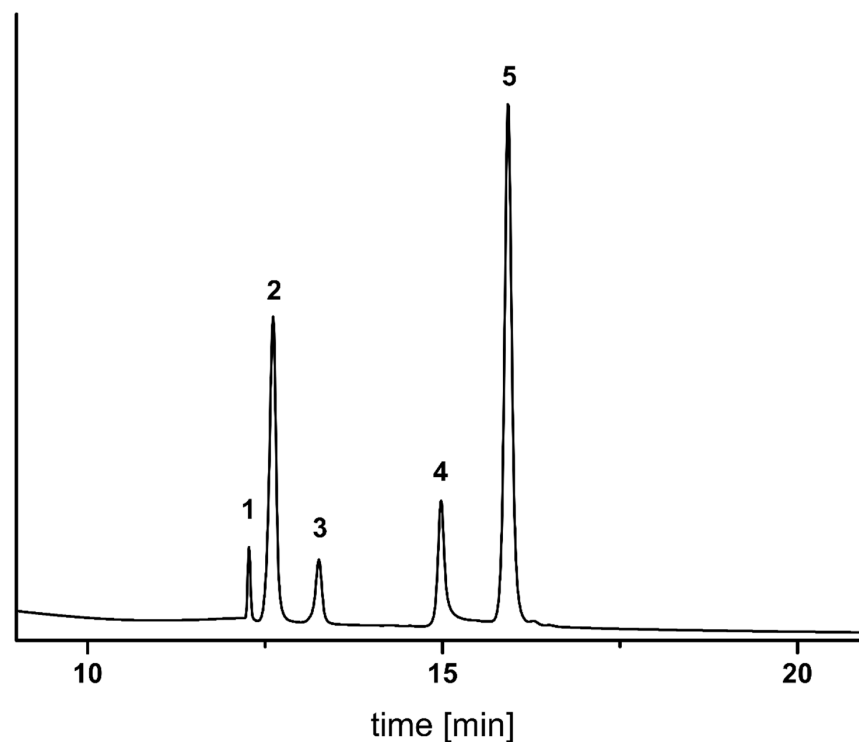


**Figure 7.** Separation of five water-soluble vitamins B<sub>1</sub> (1), B<sub>3</sub> (2), B<sub>5</sub> (3), B<sub>9</sub> (4) and B<sub>12</sub> (5). Chromatographic settings: column dimension: 250 × 4.6 mm; eluent A: H<sub>2</sub>O with 0.025 v.% TFA; eluent phase B: ACN; gradient (A/B): 5 min (100/0), 11 min (75/25), 19 min (60/40), 20 min (60/40), 21 min (100/0) and 25 min (100/0); flow: 0.8 mL · min<sup>-1</sup>; injection volume: 20 μL; column temperature: 30 °C; UV detection: 210 nm.

### 3. Materials and Methods

#### 3.1. Chemicals

Tetraethyl orthosilicate (TEOS), tetramethyl orthosilicate (TMOS) and trimethoxy (octadecyl) silane (ODTMS) were obtained from abcr GmbH (Karlsruhe, Germany). Ammonia (28–30% aqueous solution), tetrapropyl orthosilicate (TPOS) and tetrabutyl orthosilicate (TBOS) were purchased from Alfa Aesar (Schwerte, Germany). Ethanol, hydrochloric acid, 2-propanol, triethylamine and the water-soluble vitamins (B<sub>1</sub>, B<sub>3</sub>, B<sub>5</sub>, B<sub>9</sub> and B<sub>12</sub>) were bought from Sigma-Aldrich (Taufkirchen, Germany). Acetonitrile (ACN), trifluoro acetic acid (TFA) and water (all HPLC grade) were purchased from Fisher Scientific (Schwerte, Germany). Toluene and deionized water were cleaned using a solvent purification system. The test mixture (uracil, phenol, *N,N*-diethyl-*m*-toluamide and toluene) for column characterization was provided by Dr. Maisch HPLC, (Ammerbuch, Germany).

#### 3.2. Characterization

For the evaluation of the morphology, particle size and dispersity, SEM images were acquired using a Hitachi SU8030 (Krefeld, Germany). The mean particle diameter was obtained by calculating at least 400 particles from SEM images and is expressed in  $\mu\text{m}$ . The pore parameters of the materials are determined by nitrogen adsorption on a BELSORP MiniX from Microtrac Retsch GmbH (Haan, Germany). The sample preparation was carried out on a BELSORP VACII (Microtrac Retsch GmbH, Haan, Germany). For that, the silica materials were heated for 3 h at 300 °C, and a vacuum of  $2 \times 10^{-2}$  mbar was used to remove possible physisorbed residues and to achieve a reproducible equilibrium [43]. Adsorption and desorption isotherms were performed at 77 K. For the determination of the specific surface area, the adsorption isotherms were evaluated by the Brunauer–Emmet–Teller (BET) method, and for the pore volume (single point measurement at  $p/p_0 = 0.95$ ) and pore size distributions, the desorption isotherms were evaluated by the Barrett–Joyner–Halenda (BJH) method using BELMaster 7 software [44,45]. The amount of SiO<sub>2</sub> was determined after thermogravimetric measurements on a Mettler Toledo TGA/DSC. Samples were weighed in an aluminum vessel and measured at a heating rate of 5 K min<sup>-1</sup> and synthetic air (50 mL min<sup>-1</sup>).

Analytical high-performance liquid chromatography of water-soluble vitamins was performed on an Agilent 1100 series system from Agilent Technologies (Waldbronn, Germany), which consisted of a quaternary pump with degasser, an autosampling system, a column oven and a diode array detector. Instrument control, data acquisition and automated data analysis was performed by the OpenLAB CDS (Rev. C.01.07 SR3 software, Agilent Technologies, Waldbronn, Germany). A running gradient of eluent A consisting of water and 0.025 v.% TFA to eluent B consisting of acetonitrile was used according to Heudi et al. [42] The vitamins B<sub>1</sub>, B<sub>5</sub> and B<sub>12</sub> (1 mg mL<sup>-1</sup>), B<sub>3</sub> (0.5 mg mL<sup>-1</sup>) and B<sub>9</sub> (2 mg mL<sup>-1</sup>) were dissolved in water.

#### 3.3. Syntheses

Monodisperse porous *p*(GMA-*co*-EDMA) particles were prepared by a seed suspension polymerization of glycidyl methacrylate and ethylene glycol dimethacrylate in the presence of monodisperse polystyrene particles ( $1.5 \pm 0.1 \mu\text{m}$ , Figure S1, Supporting Information) [35,36,46]. Then, the *p*(GMA-*co*-EDMA) particles were functionalized with TEPA according to previous reports (for details, see Supporting Information, Figures S1–S3 [36,38,39]) to generate P@TEPA template particles. A nitrogen content of 2.4% and spectroscopic analysis indicate successful functionalization.

##### 3.3.1. Preparation of Monodisperse Porous Hybrid Beads (HB1a-f and HB2a-d) and Mesoporous Silica Microspheres (MPSM1a-f and MPSM2a-d)

Method 1: An amount of 1 g of P@TEPA particles was dispersed in a mixture of 60 mL of 2-propanol and 7.5 mL of H<sub>2</sub>O. Then, 2.4 mL of TMOS (a), TEOS (b), TPOS (c) and TBOS

(d) and 0.2 mL of an aqueous ammonia solution (28–30%) was added, and the mixture was stirred at 200 rpm for 24 h to produce hybrid beads **HB1a-d** (Table 1).

The hybrids **HB1e-f** were produced after 2.4 mL of TEOS and 1.5 mL of TMOS (e) or TPOS (f) and 0.2 mL of an aqueous ammonia solution (28–30%) were added to a dispersion of 1 g P@TEPA particles in 60 mL of 2-propanol and 7.5 mL of H<sub>2</sub>O. The mixture was stirred at 200 rpm for 24 h (Table 1).

Method 2: An amount of 1 g of P@TEPA particles was dispersed in 67.5 mL of H<sub>2</sub>O. Then, 2.4 mL of the corresponding alkoxy silane was added, and the mixture was stirred at 200 rpm. After 24 h, 0.2 mL of an aqueous ammonia solution (28–30%) was added, and the reaction was stirred for further 24 h at 200 rpm to produce hybrid beads **HB2a-d** (Table 1).

All hybrid beads were separated from their solutions, washed three times with EtOH and three times with H<sub>2</sub>O, and dried at 65 °C for 16 h. The resulting hybrid beads were calcinated at 600 °C for 10 h to provide the corresponding mesoporous silica microspheres **MPSMs** (Table 1).

### 3.3.2. Octadecyl Functionalization of Mesoporous Silica Microspheres for Chromatographic Measurements

An amount of 5 g of silica particles **MPSM1b** was dispersed in 600 mL of hydrochloric acid (3.7%) and stirred for 3 h at 100 °C (200 rpm). The particles were separated from the solution, washed with EtOH and H<sub>2</sub>O until neutral and dried at 65 °C for 16 h. The particles were then dispersed in 75 mL of toluene; 25 mL of ODTMS and 0.5 mL of triethylamine were added; and the mixture was stirred at 100 °C (200 rpm) for 6 h. The particles were separated from the solution; washed three times with toluene, three times with EtOH and twice with MeOH; and dried at 65 °C for 16 h.

The functionalized particles were packed with acetone as slurry and MeOH/H<sub>2</sub>O (85 v.%/15 v.%) as pressure medium.

## 4. Conclusions

Monodisperse mesoporous silica microspheres (MPSM) can be tailored in their sizes and pore parameters via the hard template method. This is achieved if, at the stage of the hybrid bead syntheses, the sol–gel parameters are adjusted properly. This has been successfully demonstrated here by applying a basic sol–gel process with four different alkoxy silanes in the presence of functionalized *p*(GMA-*co*-EDMA) as the template. The SNPs grow at various rates and are thus incorporated into the template pores in non-uniform sizes, which is a consequence of the different hydrolysis and condensation rates of the alkoxy silane precursors. Thus, different amounts of silica are incorporated into the template, which has an impact on the final size of the MPSM. With TMOS and TEOS as precursors, the size of the template is reproduced, while TPOS and TBOS as precursors lead to much smaller MPSMs. Moreover, the various sizes of the incorporated SNPs generate different pore parameters. The larger the SNP, the larger the pores of the MPSM, which is important for HPLC applications. The silica particles synthesized with TEOS according to Method 1 were functionalized with trimethoxy (octadecyl) silane and used as the stationary phase in HPLC. The complete baseline separation of five water-soluble vitamins was achieved with these microspheres. The robustness of the synthesis of MPSMs in their chromatographic properties was demonstrated via HPLC using three different batches with a reversed phase test mixture.

**Supplementary Materials:** The following supporting information can be downloaded at <https://www.mdpi.com/article/10.3390/ijms241411729/s1>.

**Author Contributions:** Conceptualization, A.K. and H.A.M.; methodology, F.F. and S.W.; software, J.C.S.; validation, F.F., S.W. and J.C.S.; formal analysis, F.F., S.W. and J.C.S.; investigation, F.F., S.W. and J.C.S.; resources, A.K. and H.A.M.; data curation, F.F., S.W. and J.C.S.; writing—original draft preparation, F.F.; writing—review and editing, A.K., H.A.M., J.C.S., and S.W.; visualization, F.F. and J.C.S.; supervision, A.K. and H.A.M.; project administration, A.K. and H.A.M.; funding acquisition, A.K. and H.A.M. All authors have read and agreed to the published version of the manuscript.

**Funding:** This research was funded by the Bundesministerium für Bildung und Forschung (BMBF, grant number 13FH647IX6) and the Bundesministerium für Wirtschaft und Energie (AiF/ZIM, grant number ZF4019203SL8). We acknowledge support from the Open Access Publication Fund of the University of Tübingen.

**Institutional Review Board Statement:** Not applicable.

**Informed Consent Statement:** Not applicable.

**Data Availability Statement:** Data will be made available on request.

**Acknowledgments:** We would like to thank our cooperation partner Dr. Maisch GmbH for their support in preparing the columns. We thank Elke Nadler for contributing the SEM measurements.

**Conflicts of Interest:** The authors declare no conflict of interest.

## References

1. Wang, Q.C.; Fréchet, J.M.J.; Švec, F. Reversed-phase chromatography of small molecules and peptides on a continuous rod of macroporous poly (styrene-co-divinylbenzene). *J. Chromatogr. A* **1994**, *669*, 230–235. [[CrossRef](#)] [[PubMed](#)]
2. DeStefano, J.J.; Langlois, T.J.; Kirkland, J.J. Characteristics of Superficially-Porous Silica Particles for Fast HPLC: Some Performance Comparisons with Sub-2- $\mu\text{m}$  Particles. *J. Chromatogr. Sci.* **2008**, *46*, 7. [[CrossRef](#)] [[PubMed](#)]
3. DeStefano, J.J.; Boyes, B.E.; Schuster, S.A.; Miles, W.L.; Kirkland, J.J. Are sub-2  $\mu\text{m}$  particles best for separating small molecules? An alternative. *J. Chromatogr. A* **2014**, *1368*, 163–172. [[CrossRef](#)] [[PubMed](#)]
4. Peysson, W.; Vulliet, E. Determination of 136 pharmaceuticals and hormones in sewage sludge using quick, easy, cheap, effective, rugged and safe extraction followed by analysis with liquid chromatography–time-of-flight-mass spectrometry. *J. Chromatogr. A* **2013**, *1290*, 46–61. [[CrossRef](#)]
5. Bayen, S.; Yi, X.; Segovia, E.; Zhou, Z.; Kelly, B.C. Analysis of selected antibiotics in surface freshwater and seawater using direct injection in liquid chromatography electrospray ionization tandem mass spectrometry. *J. Chromatogr. A* **2014**, *1338*, 38–43. [[CrossRef](#)]
6. Lu, Y.; Shen, Q.; Dai, Z.; Zhang, H. Multi-walled carbon nanotubes as solid-phase extraction adsorbent for the ultra-fast determination of chloramphenicol in egg, honey, and milk by fused-core C18-based high-performance liquid chromatography–tandem mass spectrometry. *Anal. Bioanal. Chem.* **2010**, *398*, 1819–1826. [[CrossRef](#)]
7. Tölgyesi, Á.; Sharma, V.K.; Fekete, J. Development and validation of a method for determination of corticosteroids in pig fat using liquid chromatography–tandem mass spectrometry. *J. Chromatogr. B* **2011**, *879*, 403–410. [[CrossRef](#)]
8. Šatinský, D.; Jägerová, K.; Havlíková, L.; Solich, P. A New and Fast HPLC Method for Determination of Rutin, Troxerutin, Diosmin and Hesperidin in Food Supplements Using Fused-Core Column Technology. *Food Anal. Methods* **2013**, *6*, 1353–1360. [[CrossRef](#)]
9. Gaborieau, M.; Castignolles, P. Size-exclusion chromatography (SEC) of branched polymers and polysaccharides. *Anal. Bioanal. Chem.* **2011**, *399*, 1413–1423. [[CrossRef](#)]
10. Schoenmakers, P.; Aarnoutse, P. Multi-Dimensional Separations of Polymers. *Anal. Chem.* **2014**, *86*, 6172–6179. [[CrossRef](#)]
11. Kirkland, J.J.; Schuster, S.A.; Johnson, W.L.; Boyes, B.E. Fused-core particle technology in high-performance liquid chromatography: An overview. *J. Pharm. Anal.* **2013**, *3*, 303–312. [[CrossRef](#)]
12. Staub, A.; Zurlino, D.; Rudaz, S.; Veuthey, J.-L.; Guilleme, D. Analysis of peptides and proteins using sub-2 $\mu\text{m}$  fully porous and sub 3- $\mu\text{m}$  shell particles. *J. Chromatogr. A* **2011**, *1218*, 8903–8914. [[CrossRef](#)]
13. Wagner, B.M.; Schuster, S.A.; Boyes, B.E.; Kirkland, J.J. Superficially porous silica particles with wide pores for biomacromolecular separations. *J. Chromatogr. A* **2012**, *1264*, 22–30. [[CrossRef](#)]
14. Badley, R.D.; Ford, W.T.; McEnroe, F.J.; Assink, R.A. Surface modification of colloidal silica. *Langmuir* **1990**, *6*, 792–801. [[CrossRef](#)]
15. Albert, K.; Brindle, R.; Martin, P.; Wilson, I.D. Characterisation of C18-bonded silicas for solid-phase extraction by solid-state NMR spectroscopy. *J. Chromatogr. A* **1994**, *665*, 253–258. [[CrossRef](#)]
16. Vrancken, K.C.; Possemiers, K.; Van Der Voort, P.; Vansant, E.F. Surface modification of silica gels with aminoorganosilanes. *Colloids Surfaces A Physicochem. Eng. Asp.* **1995**, *98*, 235–241. [[CrossRef](#)]
17. Gritti, F.; Guiochon, G. Comparative study of the performance of columns packed with several new fine silica particles. *J. Chromatogr. A* **2007**, *1166*, 30–46. [[CrossRef](#)]
18. Baker, J.S.; Vinci, J.C.; Moore, A.D.; Colón, L.A. Physical characterization and evaluation of HPLC columns packed with superficially porous particles. *J. Sep. Sci.* **2010**, *33*, 2547–2557. [[CrossRef](#)]
19. Cabooter, D.; Fanigliulo, A.; Bellazzi, G.; Allieri, B.; Rottigni, A.; Desmet, G. Relationship between the particle size distribution of commercial fully porous and superficially porous high-performance liquid chromatography column packings and their chromatographic performance. *J. Chromatogr. A* **2010**, *1217*, 7074–7081. [[CrossRef](#)]
20. Stöber, W.; Fink, A.; Bohn, E. Controlled growth of monodisperse silica spheres in the micron size range. *J. Colloid Interface Sci.* **1968**, *26*, 62–69. [[CrossRef](#)]

21. Chen, S.-L.; Dong, P.; Yang, G.-H.; Yang, J.-J. Characteristic Aspects of Formation of New Particles during the Growth of Monosize Silica Seeds. *J. Colloid Interface Sci.* **1996**, *180*, 237–241. [[CrossRef](#)]
22. Zhang, J.H.; Zhan, P.; Wang, Z.L.; Zhang, W.Y.; Ming, N.B. Preparation of monodisperse silica particles with controllable size and shape. *J. Mater. Res.* **2003**, *18*, 649–653. [[CrossRef](#)]
23. Nozawa, K.; Gailhanou, H.; Raison, L.; Panizza, P.; Ushiki, H.; Sellier, E.; Delville, J.P.; Delville, M.H. Smart Control of Monodisperse Stöber Silica Particles: Effect of Reactant Addition Rate on Growth Process. *Langmuir* **2005**, *21*, 1516–1523. [[CrossRef](#)]
24. Nakabayashi, H.; Yamada, A.; Noba, M.; Kobayashi, Y.; Konno, M.; Nagao, D. Electrolyte-Added One-Pot Synthesis for Producing Monodisperse, Micrometer-Sized Silica Particles up to 7  $\mu\text{m}$ . *Langmuir* **2010**, *26*, 7512–7515. [[CrossRef](#)]
25. Harris, M.T.; Brunson, R.R.; Byers, C.H. The base-catalyzed hydrolysis and condensation reactions of dilute and concentrated TEOS solutions. *J. Non-Cryst. Solids* **1990**, *121*, 397–403. [[CrossRef](#)]
26. Sadasivan, S.; Dubey, A.K.; Li, Y.; Rasmussen, D.H. Alcoholic Solvent Effect on Silica Synthesis—NMR and DLS Investigation. *J. Sol-Gel. Sci. Technol.* **1998**, *12*, 5–14. [[CrossRef](#)]
27. Malay, O.; Yilgor, I.; Menciloglu, Y.Z. Effects of solvent on TEOS hydrolysis kinetics and silica particle size under basic conditions. *J. Sol-Gel. Sci. Technol.* **2013**, *67*, 351–361. [[CrossRef](#)]
28. Van Blaaderen, A.; Van Geest, J.; Vrij, A. Monodisperse colloidal silica spheres from tetraalkoxysilanes: Particle formation and growth mechanism. *J. Colloid Interface Sci.* **1992**, *154*, 481–501. [[CrossRef](#)]
29. Van Helden, A.K.; Jansen, J.W.; Vrij, A. Preparation and characterization of spherical monodisperse silica dispersions in nonaqueous solvents. *J. Colloid Interface Sci.* **1981**, *81*, 354–368. [[CrossRef](#)]
30. Bogush, G.H.; Tracy, M.A.; Zukoski, C.F. Preparation of monodisperse silica particles: Control of size and mass fraction. *J. Non-Cryst. Solids* **1988**, *104*, 95–106. [[CrossRef](#)]
31. Giesche, H. Synthesis of monodispersed silica powders I. Particle properties and reaction kinetics. *J. Eur. Ceram. Soc.* **1994**, *14*, 189–204. [[CrossRef](#)]
32. Chen, K.C.; Tsuchiya, T.; Mackenzie, J.D. Sol-Gel Processing of Silica I. The role of the starting compounds. *J. Non-Cryst. Solids* **1986**, *86*, 227–237. [[CrossRef](#)]
33. Matsoukas, T.; Gulari, E. Dynamics of growth of silica particles from ammonia-catalyzed hydrolysis of tetra-ethyl-orthosilicate. *J. Colloid Interface Sci.* **1988**, *124*, 252–261. [[CrossRef](#)]
34. Han, Y.; Lu, Z.; Teng, Z.; Liang, J.; Guo, Z.; Wang, D.; Han, M.-Y.; Yang, W. Unraveling the Growth Mechanism of Silica Particles in the Stöber Method: In Situ Seeded Growth Model. *Langmuir* **2017**, *33*, 5879–5890. [[CrossRef](#)]
35. He, J.; Yang, C.; Xiong, X.; Jiang, B. Preparation and characterization of monodisperse porous silica microspheres with controllable morphology and structure. *J. Polym. Sci. A Polym. Chem.* **2012**, *50*, 2889–2897. [[CrossRef](#)]
36. Xia, H.; Wan, G.; Zhao, J.; Liu, J.; Bai, Q. Preparation and characterization of monodisperse large-porous silica microspheres as the matrix for protein separation. *J. Chromatogr. A* **2016**, *1471*, 138–144. [[CrossRef](#)]
37. Chen, J.; Zhu, L.; Ren, L.; Teng, C.; Wang, Y.; Jiang, B.; He, J. Fabrication of Monodisperse Porous Silica Microspheres with a Tunable Particle Size and Pore Size for Protein Separation. *ACS Appl. Bio Mater.* **2018**, *1*, 604–612. [[CrossRef](#)]
38. Bai, J.; Zhu, Q.; Tang, C.; Liu, J.; Yi, Y.; Bai, Q. Synthesis and application of 5  $\mu\text{m}$  monodisperse porous silica microspheres with controllable pore size using polymeric microspheres as templates for the separation of small solutes and proteins by high-performance liquid chromatography. *J. Chromatogr. A* **2022**, *1675*, 463165. [[CrossRef](#)]
39. Steinbach, J.C.; Fait, F.; Mayer, H.A.; Kandelbauer, A. Monodisperse Porous Silica/Polymer Nanocomposite Microspheres with Tunable Silica Loading, Morphology and Porosity. *Int. J. Mol. Sci.* **2022**, *23*, 14977. [[CrossRef](#)]
40. Fait, F.; Steinbach, J.C.; Kandelbauer, A.; Mayer, H.A. Impact of porosity and surface functionalization of hard templates on the preparation of mesoporous silica microspheres. *Micropor. Mesopor. Mat.* **2023**, *351*, 112482. [[CrossRef](#)]
41. Göpferich, A. Mechanisms of polymer degradation and erosion. *Biomaterials* **1996**, *17*, 103–114. [[CrossRef](#)]
42. Heudi, O.; Kiling, T.; Fontannaz, P. Separation of water-soluble vitamins by reversed-phase high performance liquid chromatography with ultra-violet detection: Application to polyvitaminated premixes. *J. Chromatogr. A* **2005**, *1070*, 49–56. [[CrossRef](#)]
43. Rouquerol, F.; Rouquerol, J.; Sing, K.S.W.; Llewellyn, P.L.; Maurin, G. *Adsorption by Powders and Porous Solids: Principles, Methodology and Applications*, 2nd ed.; Elsevier: Amsterdam, The Netherlands, 2014.
44. Lowell, S.; Shields, J.E.; Thomas, M.A.; Thommes, M. *Characterization of Porous Solids and Powders: Surface Area, Pore Size and Density*; Springer: Dordrecht, The Netherlands, 2004. [[CrossRef](#)]
45. Thommes, M.; Kaneko, K.; Neimark, A.V.; Olivier, J.P.; Rodriguez-Reinoso, F.; Rouquerol, J.; Sing, K.S.W. Physisorption of gases, with special reference to the evaluation of surface area and pore size distribution (IUPAC Technical Report). *Pure Appl. Chem.* **2015**, *87*, 1051–1069. [[CrossRef](#)]
46. Steinbach, J.C.; Fait, F.; Wagner, S.; Wagner, A.; Brecht, M.; Mayer, H.A.; Kandelbauer, A. Rational Design of Pore Parameters in Monodisperse Porous Poly(glycidyl methacrylate-co-ethylene glycol dimethacrylate) Particles Based on Response Surface Methodology. *Polymers* **2022**, *14*, 382. [[CrossRef](#)]

**Disclaimer/Publisher’s Note:** The statements, opinions and data contained in all publications are solely those of the individual author(s) and contributor(s) and not of MDPI and/or the editor(s). MDPI and/or the editor(s) disclaim responsibility for any injury to people or property resulting from any ideas, methods, instructions or products referred to in the content.